Electronic Supplementary Material (ESI) for Environmental Science: Nano.

Enhanced Sulfur Resistance by Constructing MnO_x−Co_3O_4 Interface on Ni Foam in the Removal of Benzene

Dawei Han[a], Menglan Xiao[a], Yuechang Wei[b], Xueqin Yang[d], Yucong Guo[a], Lingjuan Ma[c], Xiaolin Yu*[a], Maofa Ge[a]

[a]State Key Laboratory for Structural Chemistry of Unstable and Stable Species, Beijing National Laboratory for Molecular Sciences (BNLMS), CAS Research/Education Center for Excellence in Molecular Sciences, Institute of Chemistry, Chinese Academy of Sciences, Beijing 100190, P. R. China

[b]State Key Laboratory of Heavy Oil Processing, China University of Petroleum, Beijing 102249, P. R. China

[c]School of Chemistry and Chemical Engineering, Qufu Normal University, Qufu 273165, P. R. China

[d]College of Forestry, Henan Agricultural University, Zhengzhou 450002, P. R. China

* Email: icecoolyu@iccas.ac.cn

Content

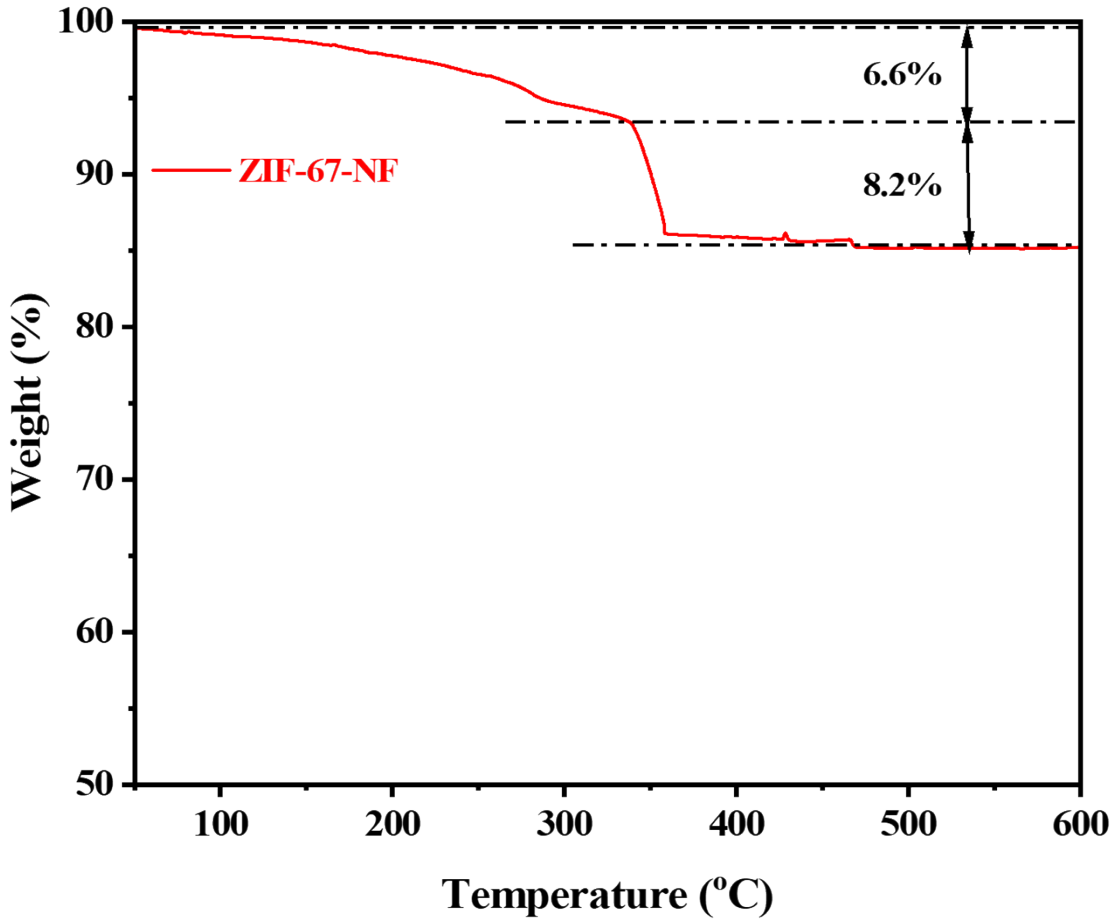

Figure S1. TG curves of ZIF-67-NF.

The TG curve of the synthesized ZIF-67-NF is shown in Figure S1. The sample was heated at a constant rate of 10 °C min^{-1} under an air flow. A weight loss of 6.6 wt % below 330 °C was attributed to the evaporation of moisture in ZIF-67. ZIF-67 decomposed rapidly and oxidated to Co_3O_4 at 330-500 °C. The total mass loss is approximately 14.8 %, affording a dark Co_3O_4-NF.

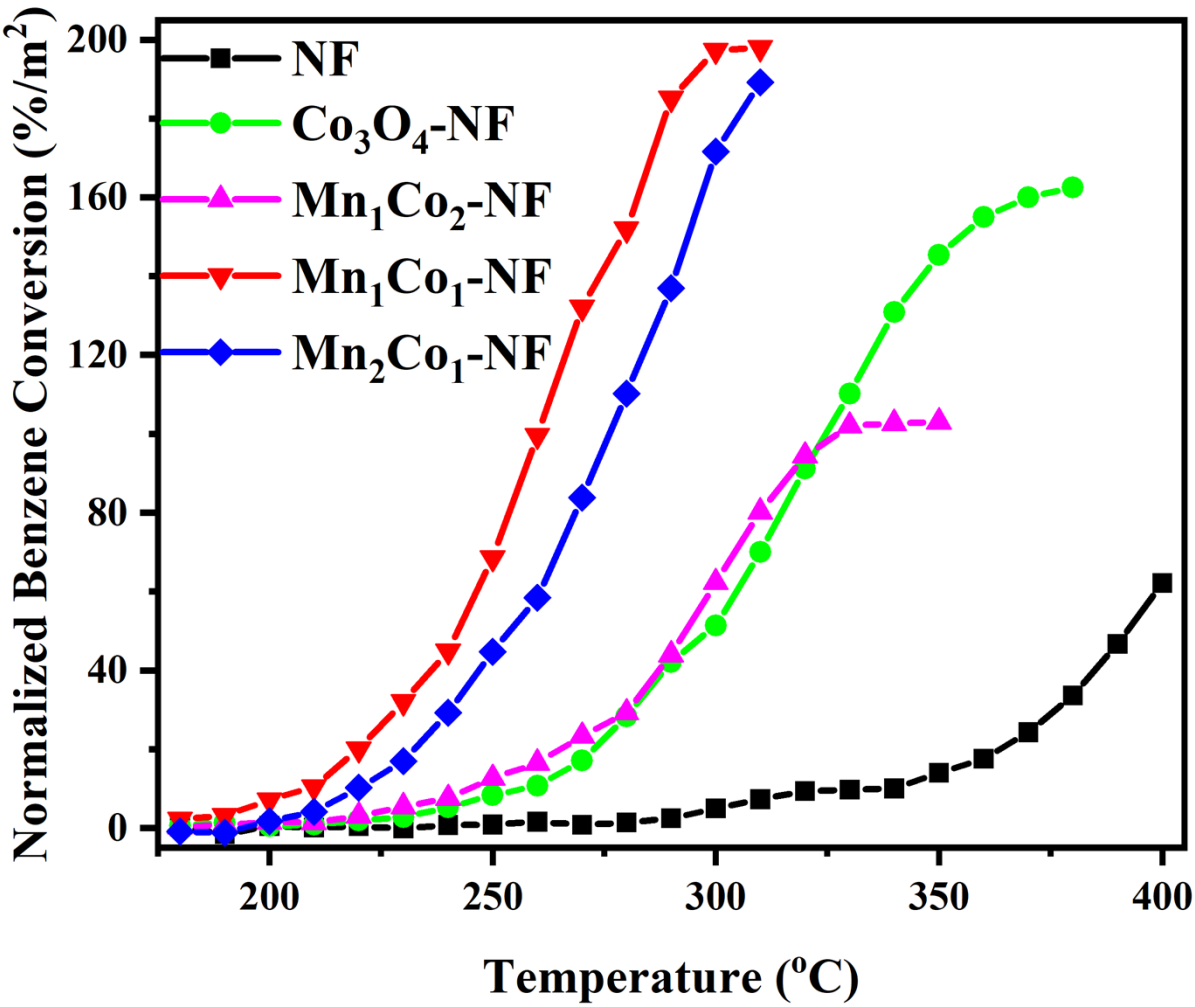

Figure S2. The conversion of Benzene per unit area over the all catalysts.

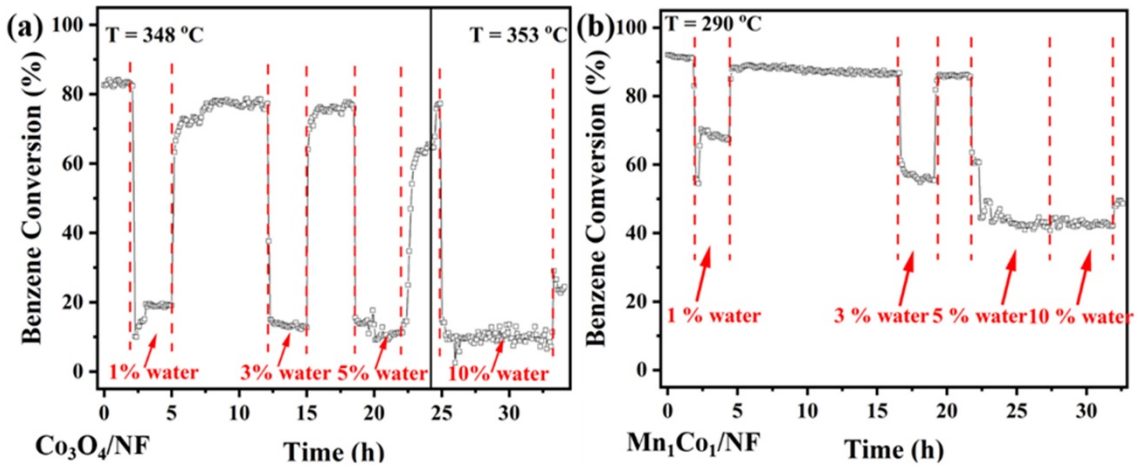

Figure S3. Water effect on Benzene conversion over Co_3O_4-NF and Mn_1Co_1-NF catalyst. (Gas composition: 100 ppm benzene, 20 % O_2, N_2 balance, and WHSV = 120000 mL g^{-1} h^{-1}).

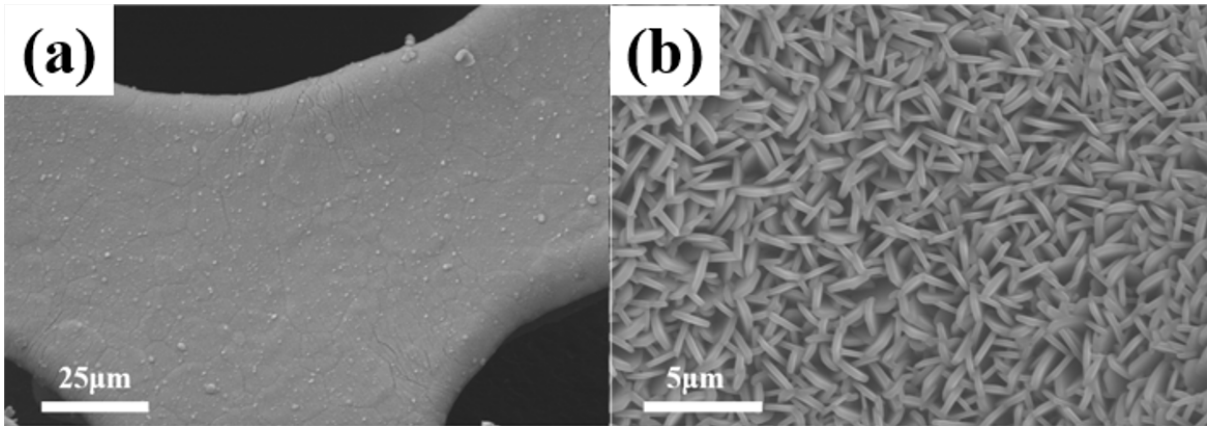

Figure S4. SEM images of the (a) NF, (b) ZIF-67-NF.

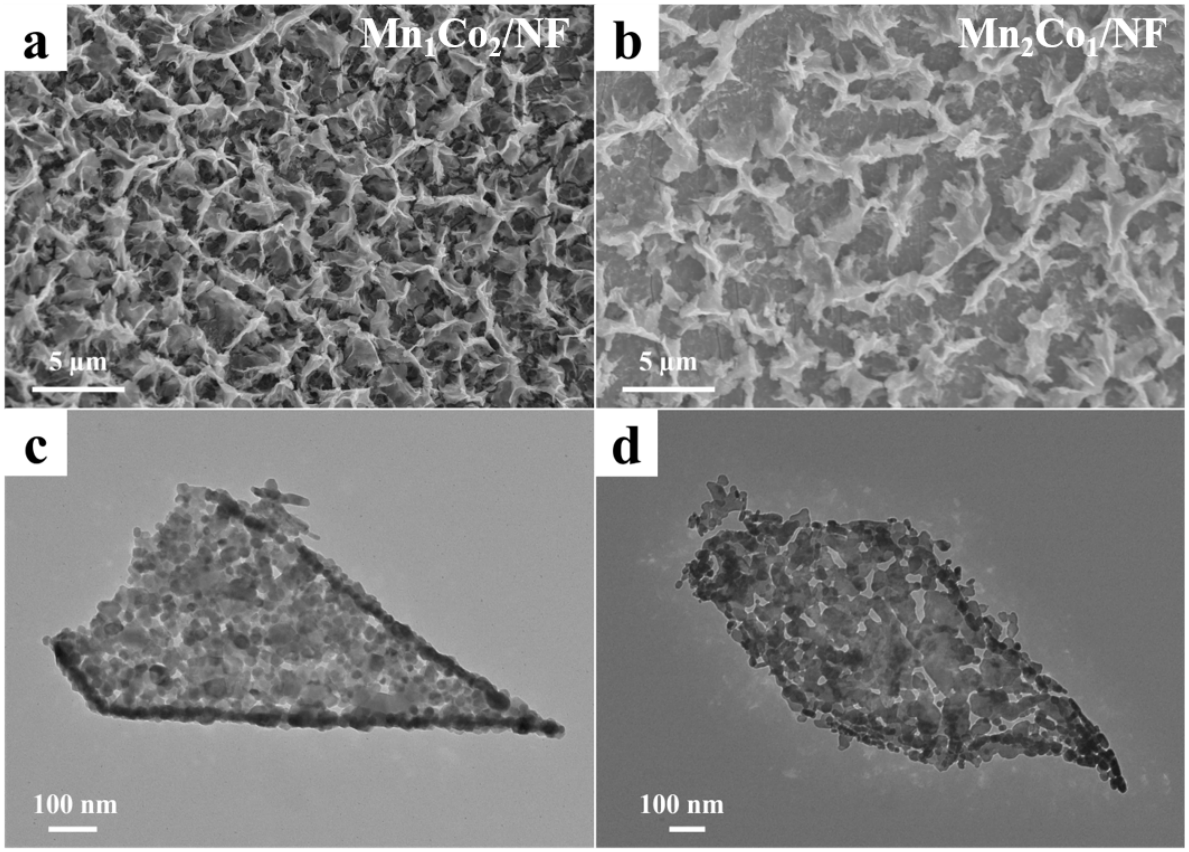

Figure S5. SEM images of the (a) Mn_1Co_2-NF catalyst and (b) Mn_2Co_1-NF catalyst; TEM images of (c) Mn_1Co_2-NF catalyst and Mn_2Co_1-NF catalyst.

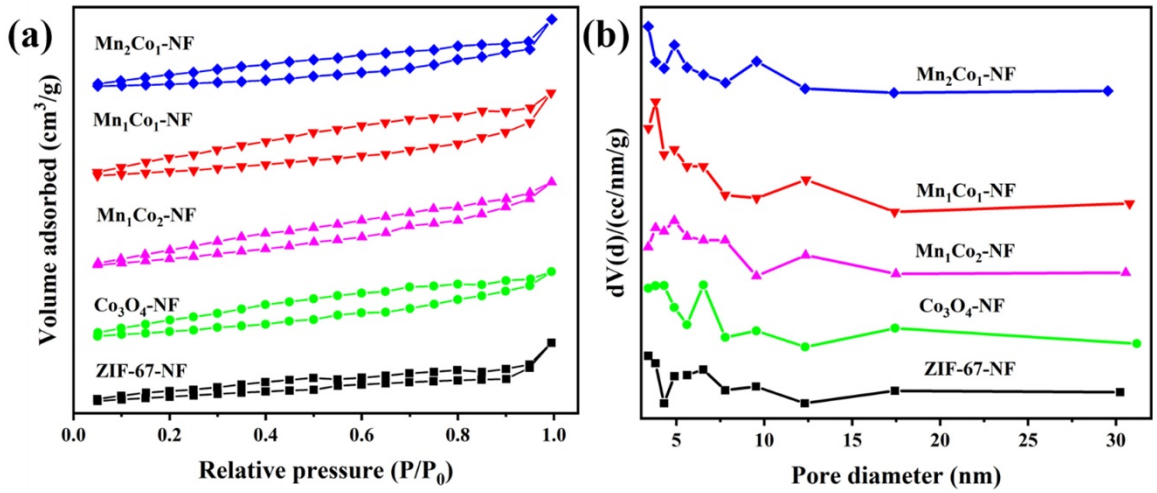

Figure S6. N_2 adsorption-desorption isotherms and pore size distributions of Co_3O_4-NF and Mn_xCo_y-NF catalysts.

The N_2 adsorption/desorption isotherms and pore size distributions of Co_3O_4-NF catalyst and Mn_xCo_y-NF catalysts were shown in Figure S7. which showed the typical type IV isotherms with a type H3 hysteresis loop for each of the samples, indicating the presence of mesopores structure in these catalysts. The specific surface areas, pore diameters and pore volume of all the catalysts were summarized in Table S1, and it could be found that the specific surface areas of the obtained samples were in the range of 10-20m^2/g. Mn_1Co_2-NF catalyst had the largest BET surface area (19.4 m^2/g), and Mn_1Co_1-NF catalyst had the lowest BET surface are (1.5 m^2/g). Therefore, the small difference in specific surface area will be not the main factor that influences the catalytic performance of catalysts.

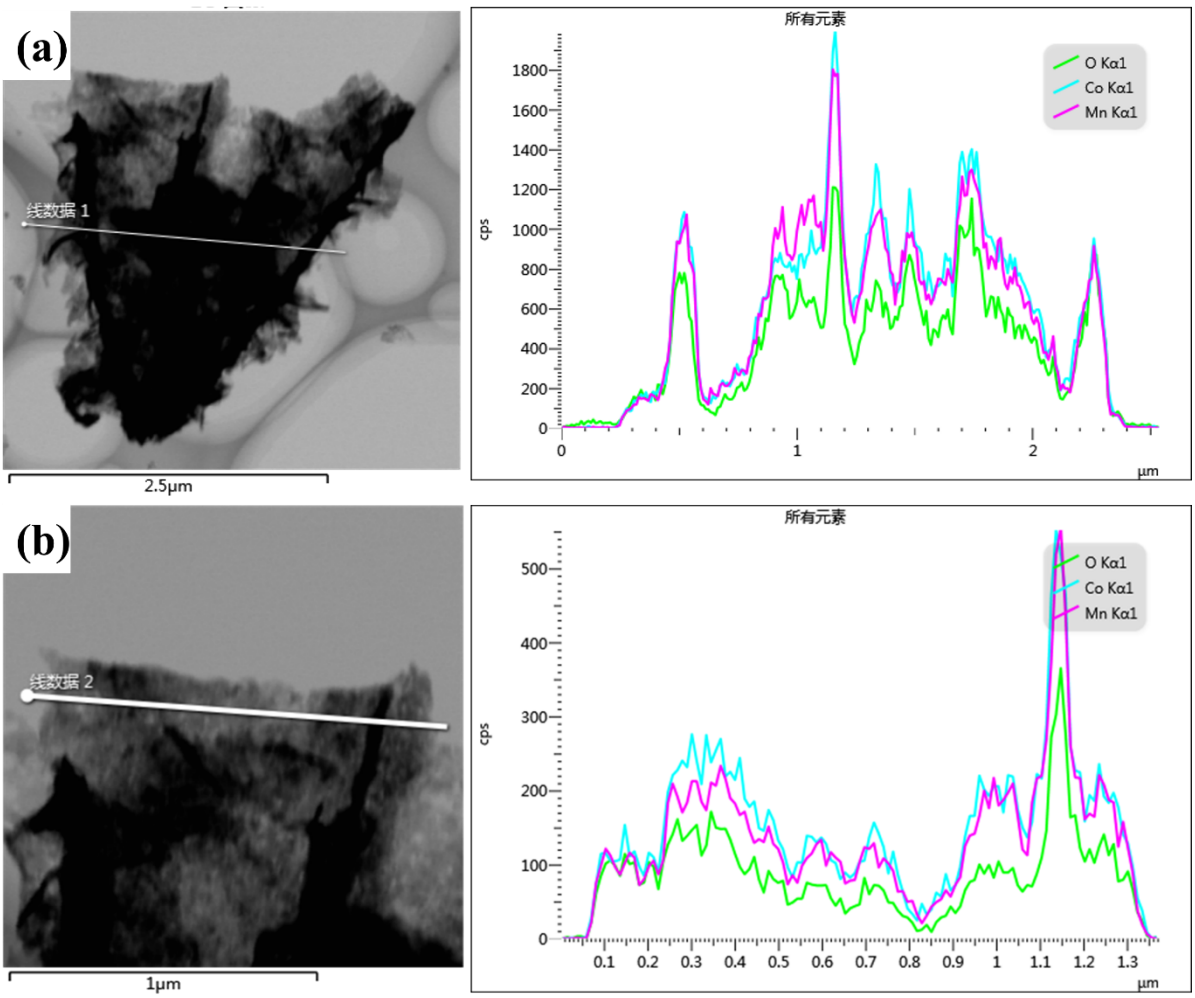

Figure S7. Line scanning image in different location of Mn_1Co_1-NF.

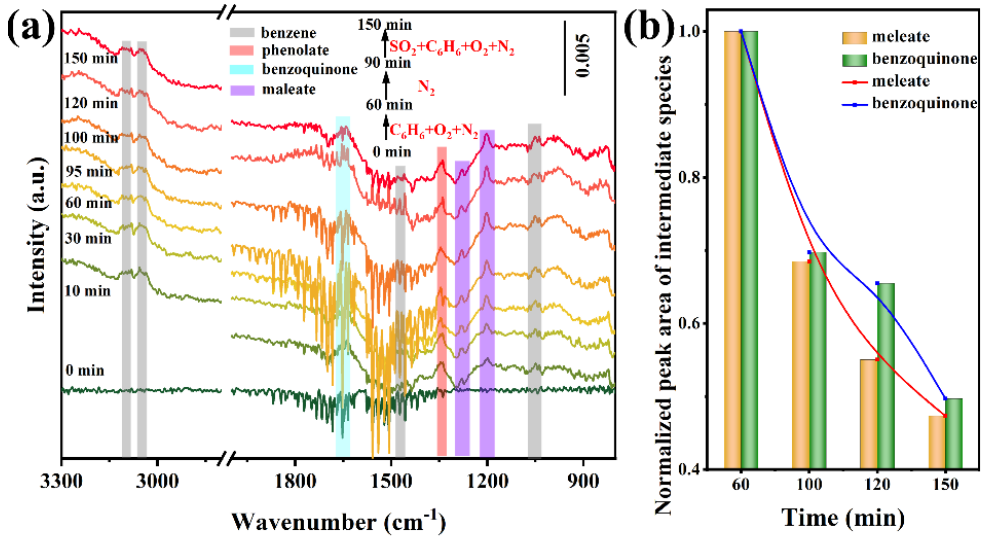

Figure S8. In situ DRIFTS spectra of reactant adsorption at 310 ºC (a) and the normalized content of reaction intermediate species (b) over Co_3O_4-NF catalyst.

For the Co_3O_4-NF catalyst, the bands at 3096, 3049 and 1048 cm^{-1} were ascribed to the C-H stretching vibration in the benzene rings[1, 2], the bands at 1630 cm^{-1} corresponded to to the C=O stretching vibrations of quinone species[3], the bands at 1202 and 1280 cm^{-1} was ascribed to the phenolate species and the bands at 1349 cm^{-1} corresponded to maleate species[3-5], which shows similar intermediate species with Mn_1Co_1-NF catalyst.

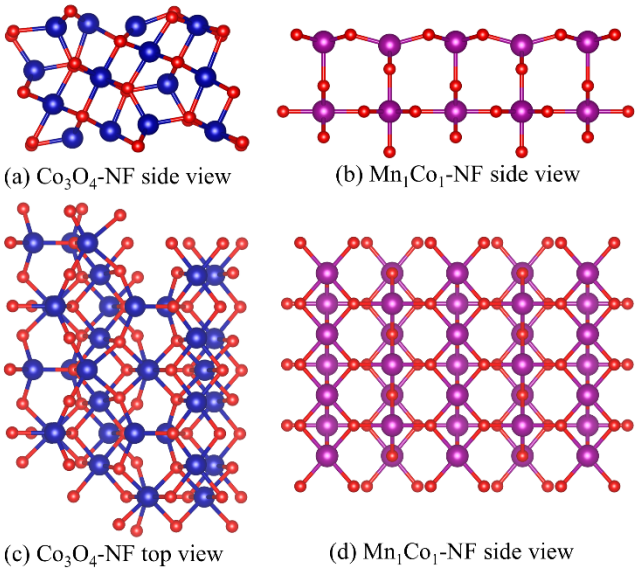

Figure S9. Side and top views of Co_3O_4-NF (a, c) and Mn_1Co_1-NF (b, d).

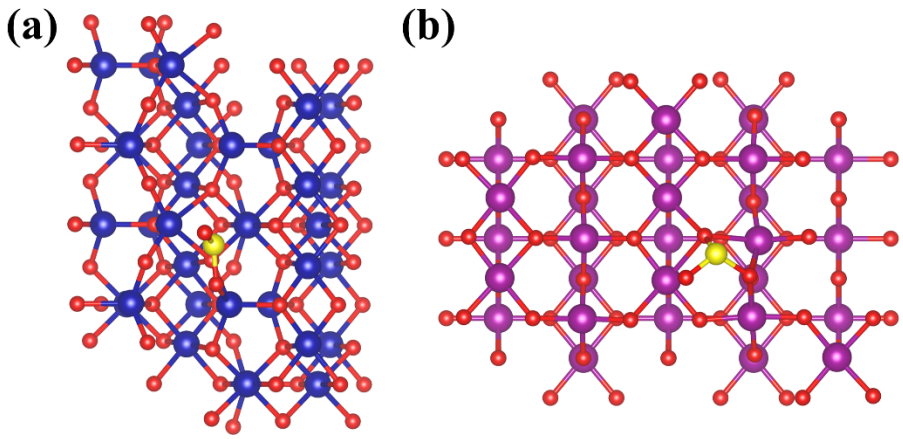

Figure S10. The top view of the SO_2-adsorbed (b) on Co_3O_4-NF and (c) Mn_1Co_1-NF.

Table S1. Physicochemical Properties of the Samples.

Samples	Surface area (m^2/g)	Total pore volume (cm^3/g)	Average pore diameter (nm)
Co_3O_4/NF	12.3	0.025	3.41
Mn_1Co_2/NF	19.4	0.032	3.82
Mn_1Co_1/NF	10.1	0.032	3.82
Mn_2Co_1/NF	1.5	0.025	3.41

1. Z. Hou, L. Dai, Y. Liu, J. Deng, L. Jing, W. Pei, R. Gao, Y. Feng and H. Dai, Highly efficient and enhanced sulfur resistance supported bimetallic single-atom palladium-cobalt catalysts for benzene oxidation, *Applied Catalysis B-Environmental*, 2021, **285**.
2. K. Yang, Y. Liu, J. Deng, X. Zhao, J. Yang, Z. Han, Z. Hou and H. Dai, Three-dimensionally ordered mesoporous iron oxide-supported single-atom platinum: Highly active catalysts for benzene combustion, *Applied Catalysis B: Environmental*, 2019, **244**, 650-659.
3. J. Lichtenberger, Catalytic oxidation of chlorinated benzenes over V2O5/TiO2 catalysts, *Journal of Catalysis*, 2004, **223**, 296-308.
4. X. Ma, M. Xiao, X. Yang, X. Yu and M. Ge, Boosting benzene combustion by engineering oxygen vacancy-mediated Ag/CeO2-Co3O4 catalyst via interfacial electron transfer, *J Colloid Interface Sci*, 2021, **594**, 882-890.
5. Y. Liang, Y. Liu, J. Deng, K. Zhang, Z. Hou, X. Zhao, X. Zhang, K. Zhang, R. Wei and H. Dai, Coupled palladium–tungsten bimetallic nanosheets/TiO2 hybrids with enhanced catalytic activity and stability for the oxidative removal of benzene, *Environmental science & technology*, 2019, **53**, 5926-5935.